JACS
JOURNAL OF THE AMERICAN CHEMICAL SOCIETY
pubs.acs.org/JACS
Article

Direct Observation of Diastereomeric α-C-Bound Enolates during Enantioselective α-Arylations: Synthesis, Characterization, and Reactivity of Arylpalladium Fluorooxindole Complexes

Eric D. Kalkman and John F. Hartwig*

Cite This: J. Am. Chem. Soc. 2021, 143, 11741−11750
Read Online

ABSTRACT: The Pd-catalyzed asymmetric α-arylation of carbonyl compounds is a valuable strategy to form benzylic stereocenters. However, the origin of the stereoselectivity of these reactions is poorly understood, and little is known about the reactivity of the putative diastereomeric arylpalladium enolate intermediates. To this end, we report the synthesis and characterization of a series of diphosphine-ligated arylpalladium fluoroenolate complexes, including complexes bearing a metal-bound, stereogenic carbon and an enantioenriched chiral diphosphine ligand. These complexes reductively eliminate to form chiral α-aryl-α-fluorooxindoles with enantioselectivities and rates that are relevant to those of the catalytic process with SEGPHOS as the ancillary ligand. Kinetic studies showed that the rate of reductive elimination is slightly slower than the rate of epimerization of the intermediate, causing the reductive elimination step to impart the greatest influence on the enantioselectivity. DFT calculations of these processes are consistent with these experimental rates and suggest that the minor diastereomer forms the major enantiomer of the product. The rates of reductive elimination from complexes containing a variety of electronically varied aryl ligands revealed the unusual trend that complexes bearing more electron-rich aryl ligands react faster than those bearing more electron-poor aryl ligands. Noncovalent Interaction (NCI) and Natural Bond Orbital (NBO) analyses of the transition-state structures for reductive elimination from the SEGPHOS-ligated complexes revealed key donor−acceptor interactions between the Pd center and the fluoroenolate fragment. These interactions stabilize the pathway to the major product enantiomer more strongly than they stabilize that to the minor enantiomer.

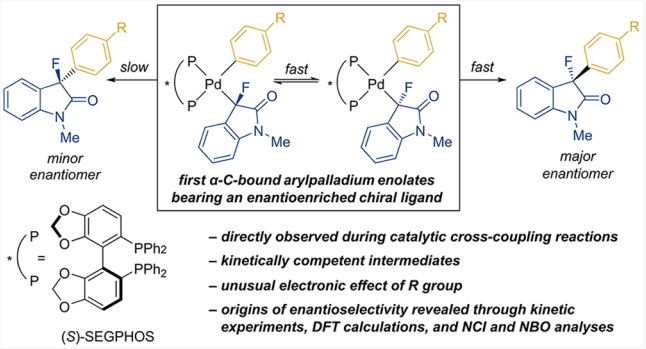

INTRODUCTION

The α-arylation of carbonyl compounds has become a widely practiced class of coupling reactions, and enantioselective versions of this process have been reported in both intermolecular and intramolecular forms with a range of carbonyl compounds and sp^2-electrophiles.[1−26] The intermediates in the α-arylations that form the carbon−carbon bond are C-bound arylpalladium enolate complexes. Examples of arylpalladium enolate complexes have been prepared, and the rates of reductive elimination as a function of the steric and electronic properties of the enolate have been studied.[6,27,28] However, analogous enolate complexes that are putative intermediates in the enantioselective processes and that undergo reductive eliminations to form enantioenriched, chiral products have not been studied. Thus, the influence of the chiral ancillary ligand and enolate structure on the formation, speciation, and reactivity of diastereomeric arylpalladium enolate intermediates is unknown.

In particular, it is unknown whether formation of the C-bound arylpalladium enolate complexes (Figure 1, red) or reductive elimination from these complexes (Figure 1, blue) is the stereochemistry-determining step in the enantioselective formation of chiral products (eq 1). This information has

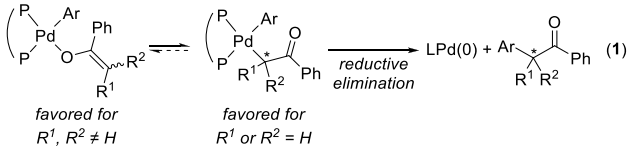

been difficult to obtain because α,α-disubstituted enolates typically bind to the metal center through the enolate oxygen (eq 1; R^1, $R^2 \neq H$), not the α-carbon (R^1 or R^2 = H).[6,27−29] This preference for κO binding over κC binding precludes the evaluation of diastereomeric intermediates because the C-bound

Received: May 24, 2021
Published: July 26, 2021

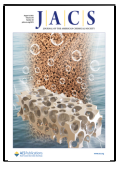

https://doi.org/10.1021/jacs.1c05346
J. Am. Chem. Soc. 2021, 143, 11741−11750

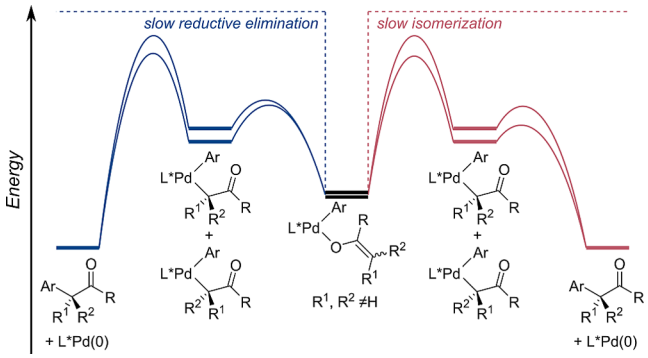

Figure 1. Conceptual energy diagram of possible epimerizations and stereochemistry-determining steps of the formation of enantioenriched α-aryl carbonyl compounds from chiral arylpalladium α,α-disubstituted enolate complexes.

form is not observed. Diastereomeric C-bound enolate complexes of α-monosubstituted carbonyl compounds might be observable because the α-C-bound isomer of these complexes can be more stable than the O-bound form.[27] However, the benzylic α-C−H bond in the coupled products is more acidic than the α-C−H bonds of the starting carbonyl compounds, and this greater acidity of the product complicates analysis of the origins of enantioselectivity because racemization of the arylated products occurs under the basic reaction conditions typically employed for catalysis.[9,16,30−34] Thus, information on the origins of enantioselectivity has been limited to that from computational studies.[32,33]

We recently reported several examples of the enantioselective α-arylation of α-fluoroenolates.[18,19] We considered that these reactions might provide an opportunity to observe such diastereomeric intermediates because the fluorine atom on these enolates could lead to an electronic preference for the α-C-bound form[35−37] and the small size of fluorine would not significantly destabilize this form due to steric interactions. Because the arylated products formed from these reactions lack acidic C−H bonds at the newly formed stereocenter, they do not epimerize under catalytic conditions.[18,19] Thus, such systems provide a potential opportunity to study the reactivity of enolate complexes containing a stereogenic, palladium-bound carbon atom and a chiral ancillary phosphine ligand and to address whether the formation of these diastereomeric complexes or the reductive elimination from these complexes determines enantioselectivity.

We report the synthesis of diphosphine-ligated, chiral, arylpalladium fluoroenolate complexes derived from an α-fluorooxindole in which the enolate fragments are bound to the Pd center at a stereogenic α-carbon, including the first such complexes bearing a chiral diphosphine ligand ((*S*)-SEGPHOS). These complexes undergo reductive elimination in high yields, allowing an assessment of the relative rates of epimerization of and reductive elimination from the fluoroenolate complexes. These studies show that the fluoroenolate complexes undergo epimerization with rates that are comparable to, but slightly faster than, those of reductive elimination and that reductive elimination is the principal determinant of enantioselectivity. Studies of analogous complexes containing the achiral ligand DPPF (DPPF = (1,1′)-bis-(diphenylphosphino)ferrocene enabled comparisons to prior studies of fluorinated and nonfluorinated arylpalladium enolate, and allowed further information on the electronic effects of the aryl fragment on the rates of reductive elimination to be obtained.

RESULTS AND DISCUSSION

1. Synthesis and Reactivity of (*S*)-SEGPHOS-ligated Arylpalladium Fluoroenolate Complexes. Our investigations began with the preparation of (*S*)-SEGPHOS-ligated arylpalladium fluorooxindole species that are the putative intermediates that undergo reductive elimination to form the coupled products in our previous studies on the Pd-catalyzed α-arylation of 3-fluorooxindoles.[19] Complexes **2a** and **2b** were prepared by treating arylpalladium bromide complexes **1a−b** with KO*t*Bu in THF to form the corresponding arylpalladium *tert*-butoxide complexes, which were combined *in situ* with 3-fluoro-*N*-methyl-oxindole (**3**) to form the desired fluoroenolate complexes as mixtures of diastereomers (Scheme 1). The

Scheme 1. Preparation of (*S*)-SEGPHOS-ligated Arylpalladium Fluorooxindole Complexes 2a−b

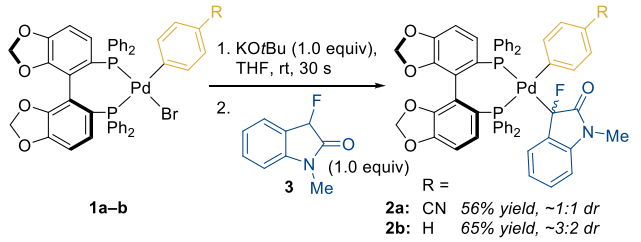

diagnostic NMR signals of (4-cyanophenyl)palladium enolate complex **2a** are shown in Figure 2. The ^{19}F NMR spectra of both complexes **2a** and **2b** consist of two doublets of doublets with large coupling constants ($^{3}J_{F-P}$ = 112−115 Hz and 38−39 Hz), each of which are coupled to a pair of doublets of doublets in the ^{31}P{^{1}H} NMR spectra ($^{2}J_{P-P}$ = 27−33 Hz). These data are

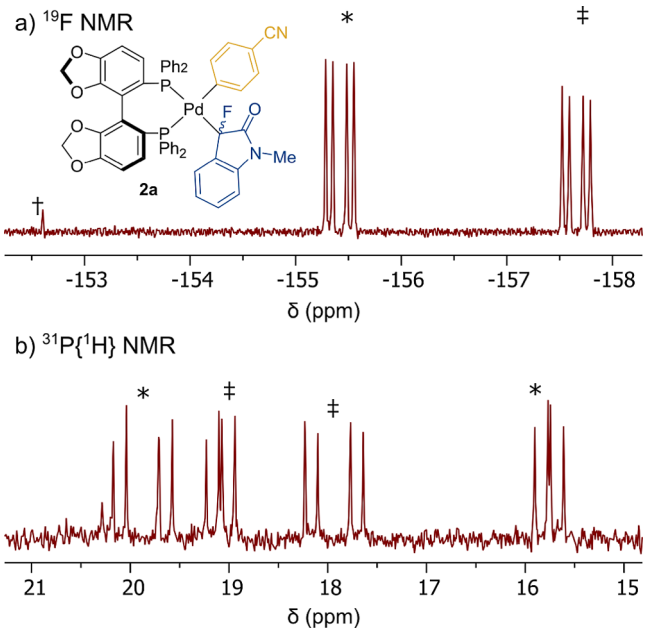

Figure 2. Diagnostic signals of **2a** in its (a) ^{19}F and (b) ^{31}P{^{1}H} NMR spectra (C_6D_6). (*) and (‡) indicate peaks corresponding to the two diastereomers of **2a**. (†) indicates a trace amount of the coupled product **4a**.

https://doi.org/10.1021/jacs.1c05346
J. Am. Chem. Soc. 2021, 143, 11741−11750

consistent with a mixture of diastereomeric α-C-bound enolate complexes containing a fluorine atom on the α-carbon.

Heating complexes **2a–b** at 65 °C in C_6D_6 in the presence of PPh_3 to trap the generated Pd(0) species resulted in the quantitative formation of the α-arylated products **4a–b** in high *ee*'s (93% and 95% for **4a** and **4b**, respectively; see Table 1). Both

Table 1. Reductive Elimination from (*S*)-SEGPHOS-ligated Arylpalladium Fluoroenolate Complexes 2 at 65 °C

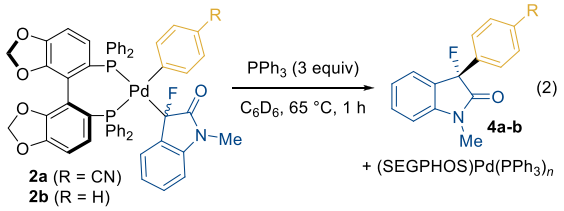

Complex	R	k_{obs} ($s^{-1}\times10^4$)[a]	*dr*[b]	Yield	*ee* of 4
2a	CN	8.6 ± 0.4	3.0:1	>99%	93%
2b	H	26 ± 2	3.2:1	>99%	95%

[a]Determined by monitoring the rate of formation of coupled product by $^{19}F\{^{31}P\}$ NMR spectroscopy. [b]Determined as the average ratio between the two diastereomers (major:minor) during the second half-life of the reaction.

the formation of arylated products **4a–b** and the decomposition of the starting complexes **2a–b** were monitored by quantitative inverse-gated $^{19}F\{^{31}P\}$ NMR spectroscopy and displayed clean first-order kinetics.

The time course for the decomposition of **2a** and formation of **4a** is shown in Figure 3a. For both complexes **2a** and **2b**, the

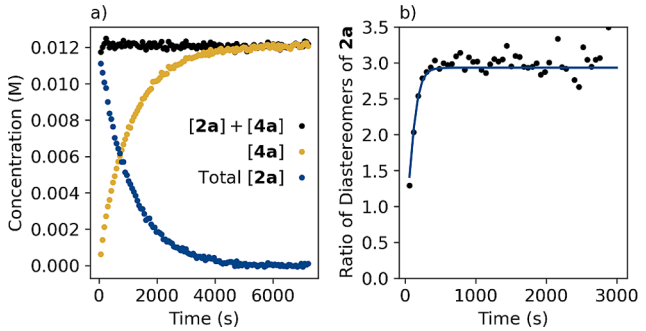

Figure 3. Time courses of the thermolysis of **2a** in C_6D_6 at 65 °C (eq 2) showing (a) the concentrations of **2a** and **4a** and (b) the *dr* of **2a**. Concentrations were determined by quantitative inverse-gated $^{19}F\{^{31}P\}$ NMR spectroscopy relative to an internal standard. The solid line in part b represents the simulated *dr* of **2a** according to the fitted rate constants for epimerization and thermolysis (see text).

concentrations of the two diastereomers quickly reached a ratio of ~3:1, and this ratio remained constant over the remainder of the reaction. While the *dr* of the unsubstituted phenylpalladium enolate complex **2b** reached its equilibrium ratio within the first minute of heating (see the SI), the isomerization of (4-cyanophenyl)palladium enolate complex **2a** to its steady-state *dr* was slow enough to observe over the first 5 min of the reaction (Figure 3b). Because the *ee*'s of the coupled products **4a–b** far exceeded the steady-state *dr*'s of the fluoroenolate complexes **2a–b**, the relative rates of reductive elimination from the two diastereomers must be the dominant contributor to the enantioselectivity of this reaction.[38]

To obtain a more complete picture of the dynamics of the reaction of **2a**, we estimated the first-order rate constants for the epimerization of and the reductive elimination from **2a** using the kinetic modeling software COPASI (Scheme 2; see the SI for a

Scheme 2. Rate Constants[a] of Epimerization and Reductive Elimination of Complex 2a as Modeled by COPASI[39]

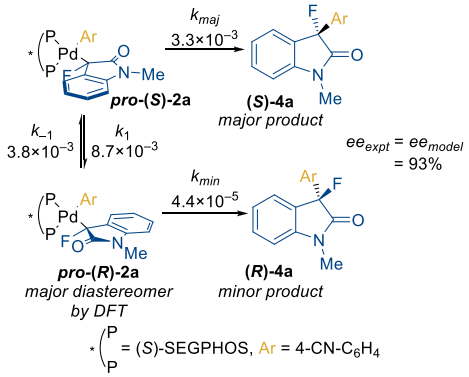

[a]Rate constants are given in units of s^{-1}. Assignment of major and minor diastereomers of **2a** was based on DFT calculations (*vide infra*).

derivation of the rate equation).[39] While isomerization from the diastereomer that gives the major product enantiomer (***pro*-(*S*)-2a**) to the diastereomer that gives the minor product enantiomer (***pro*-(*R*)-2a**) occurs with a rate constant that is significantly larger than that of the subsequent reductive elimination step by more than 2 orders of magnitude ($k_1 = 8.7\times10^{-3}$ s^{-1} *vs* $k_{min} = 4.4\times10^{-5}$ s^{-1}, respectively), isomerization of the diastereomer that gives the minor product to the diastereomer that gives the major product is just barely faster than the rate of reductive elimination ($k_{-1} = 3.8\times10^{-3}$ s^{-1} *vs* $k_{maj} = 3.3\times10^{-3}$ s^{-1}, respectively). These similar rate constants for epimerization and reductive elimination are consistent with the sluggish equilibration observed in Figure 3b and highlight the large difference in rates between the two manifolds forming the two enantiomeric products. Computational modeling of the individual isomerization and reductive elimination steps by DFT, along with a discussion of the implications for the origins of enantioselectivity, are presented in Section 3 and in the Conclusion.

2. Analysis of the Electronic Effect of the Eliminating Aryl Fragment. Because the rates of reductive elimination can depend on the electronic properties of the eliminating aryl group, causing the electronic properties to affect the relative rates for reductive elimination and epimerization, we also compared the rates of reductive elimination from unsubstituted **2b** and *para*-CN-substituted **2a**. Surprisingly, the formation of arylated **4b** from the complex containing the more electron-rich phenyl group (**2b**) occurred ~3 times faster than the formation of **4a** from the complex containing the more electron-poor 4-cyanophenyl group (**2a**). This difference is the opposite of that observed for the rates of reductive elimination from diphosphine-ligated arylpalladium complexes of nonfluorinated enolates and most Pd-catalyzed reductive elimination reactions to form C–X bonds.[28] Such rates are generally faster for complexes containing more electron-poor aryl groups than for complexes containing more electron-rich aryl groups.[40–43]

Two studies on the electronic effect of the aryl ligand on the rates of reductive elimination of arylpalladium(II) difluoromethyl[44] and difluoroenolate[45] complexes showed that

https://doi.org/10.1021/jacs.1c05346
J. Am. Chem. Soc. 2021, 143, 11741–11750

elimination occurs more rapidly from complexes containing more electron-donating aryl groups than from complexes containing less electron-donating aryl groups. Our data imply that this trend observed previously for two classes of fluoroalkyl complexes is general for a range of fluoroenolates.

In light of these results, we sought to explore further the influence of the electronic properties of the Pd-bound aryl group on the rates of reductive elimination in the absence of potentially competing stereoelectronic effects from the two diastereomers of the SEGPHOS-ligated complexes **2a–b**. To this end, we prepared a series of DPPF-ligated arylpalladium fluorooxindole complexes **6a–g** (DPPF = 1,1′-bis(diphenylphosphino)-ferrocene). These complexes were prepared from the analogous arylpalladium bromide complexes **5a–g** by a route analogous to that used to prepare SEGPHOS-ligated complexes **2a–b** (Scheme 3). The ^{19}F NMR spectra of complexes **6a–g** consist

Scheme 3. Preparation of DPPF-ligated Arylpalladium Fluorooxindole Complexes 6a–g

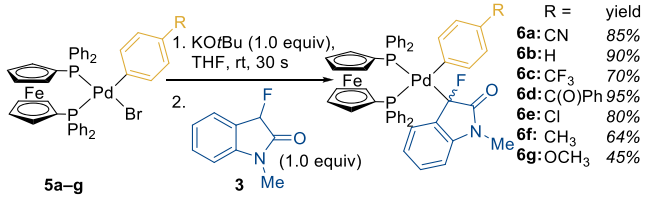

of a single doublet of doublets ($^3J_{F-P}$ ~ 110–112, 39–40 Hz) coupled to two doublets of doublets in the $^{31}P\{^1H\}$ spectra. These data indicate that the enolates in these complexes are connected to palladium through the α-carbon of the enolate.

We also unambiguously confirmed the α-C-bound connectivity of (4-cyanophenyl)palladium enolate complex **6a** in the solid state by single crystal X-ray diffraction (Figure 4). The

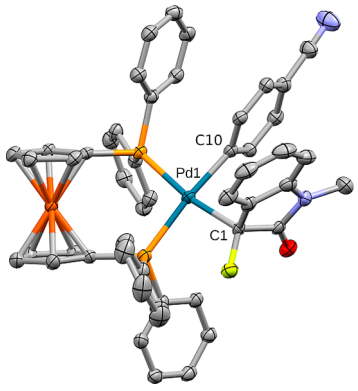

Figure 4. Thermal ellipsoid drawing of fluoroenolate complex **6a**. Ellipsoids are drawn at 50% probability, and hydrogens and crystallization solvent are omitted for clarity. Teal = Pd, light gray = C, blue = N, light green = F, light orange = P, dark orange = Fe. Selected bond lengths: Pd–C1, 2.139(3) Å; Pd–C10, 2.063(3) Å.

Pd–C(aryl) bond of **6a** is slightly longer than Pd–C(aryl) bonds of previously reported DPPF-ligated arylpalladium fluoroenolate complexes (2.063(3) Å; literature: 2.051(2)–2.058(3) Å).[45] The Pd–C(enolate) bond (2.139(3) Å) of **6a** is longer than the Pd–C(enolate) bonds of mono- and difluoroester complexes (2.105(3) Å and 2.099(3) Å, respectively), but is shorter than that of a difluoroamide complex (2.188(3) Å).

Heating the enolate complexes **6a–g** in C_6D_6 at 80 °C in the presence of PPh_3 afforded the corresponding arylated fluorooxindoles in quantitative yields. The reactions were monitored by quantitative inverse-gated $^{19}F\{^{31}P\}$ NMR spectroscopy, and the rate constants were determined from first-order exponential fits of product formation (see the SI for a table of rate constants). A Hammett plot of the relative rate constants of reductive elimination vs the σ_p[46] substituent parameter of the R group on the aryl ring is shown in Figure 5. In contrast to

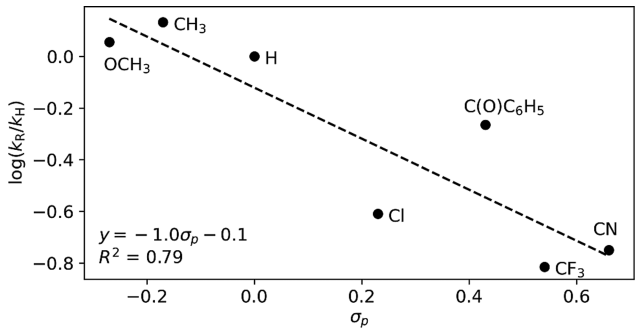

Figure 5. Hammett plot of the relative rates of thermolysis of complexes **6a–g** vs the σ_p parameter of the para substituent of the eliminating aryl group. See the SI for a table of rate constants.

previous studies on arylpalladium enolate complexes that did not contain fluorine,[28,43] the reductive elimination from fluoroenolate complexes **6a–g** containing more electron-donating aryl fragments were faster than those of complexes containing more electron-withdrawing aryl fragments (ρ = −1.0), with the electron-rich *para*-methyl-substituted complex **6f** reacting ~8 times faster than the electron-poor *para*-CF_3-substituted complex **6c**. This trend matches that observed for SEGPHOS-ligated complexes **2a–b** and that for the limited previous arylpalladium fluoroenolates shown to undergo reductive elimination,[44,45] giving more evidence for the unusual effect of fluorine on the rates of reductive elimination.

To identify parameters that increase the linearity of the Hammett plot in Figure 5, we also constructed a composite substituent parameter $\bar{\sigma}$ by varying the inductive ("field") and resonance contributions of the R group on the aryl ligand (see Figure S8 and the preceding discussion in the SI). Such a treatment previously increased the linearity of the fits of the relative rates of reductive elimination reactions of arylpalladium amide,[40] thiolate,[41] and alkoxide complexes.[42,47] However, the optimal combination of field and resonance parameters ($\bar{\sigma}$ = 0.69 F + 0.31 F) only modestly increased the linearity (R^2 = 0.87) of the Hammett plot for reductive elimination from complexes **6a–g**.

3. Computational Modeling and Origins of Enantioselectivity. DFT calculations of the energies of the α-C and O-bound enolates of (*S*)-SEGPHOS-ligated arylpalladium fluoroenolate complexes **2a–b** are consistent with the observation of the C-bound connectivity in the ground state (Figure 6; see the SI for computational methods, structures, and energies). For both 4-cyanophenyl complex **2a** and phenyl complex **2b**, the free energy of the diastereomer that affords the minor enantiomer (***pro*-(*R*)**) was found to be lower than that of the complex that affords the major enantiomer (***pro*-(*S*)**) for several functionals (ΔG = 0.8–1.3 kcal/mol; see Table S4 in the SI). The energies of the energy-minimized O-bound isomers of complexes **2a** and **2b** were calculated to be more than 4 kcal/mol higher than the

https://doi.org/10.1021/jacs.1c05346
J. Am. Chem. Soc. 2021, 143, 11741–11750

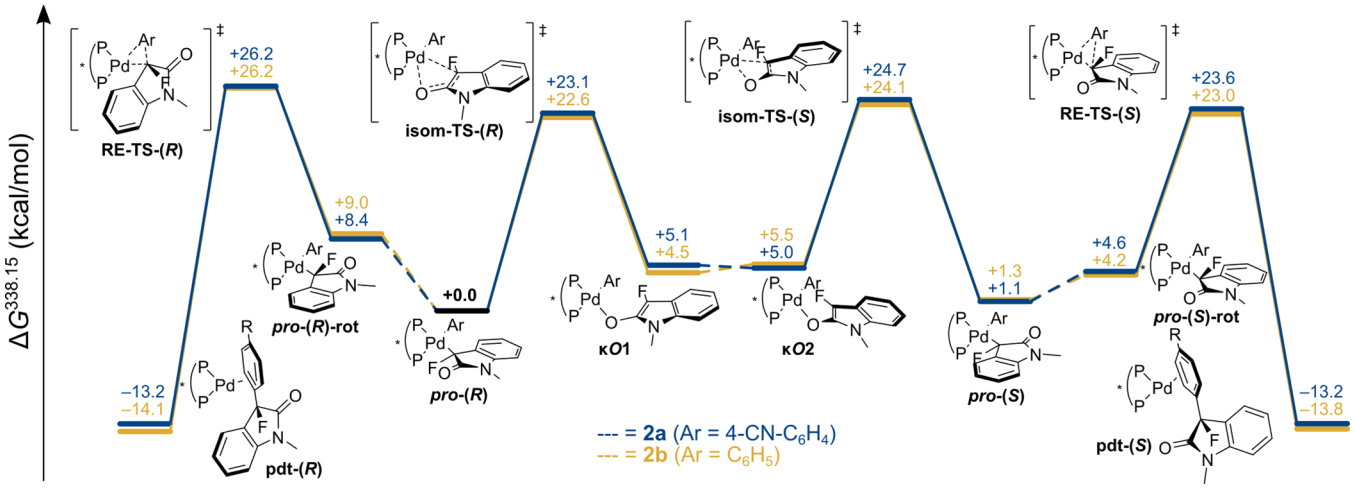

Figure 6. Energy coordinate diagram for the epimerization of and reductive elimination from (*S*)-SEGPHOS-ligated arylpalladium complexes **2a**–**b**. Free energies are given at 338.15 K in kcal/mol. See the SI for computational methods and structures.

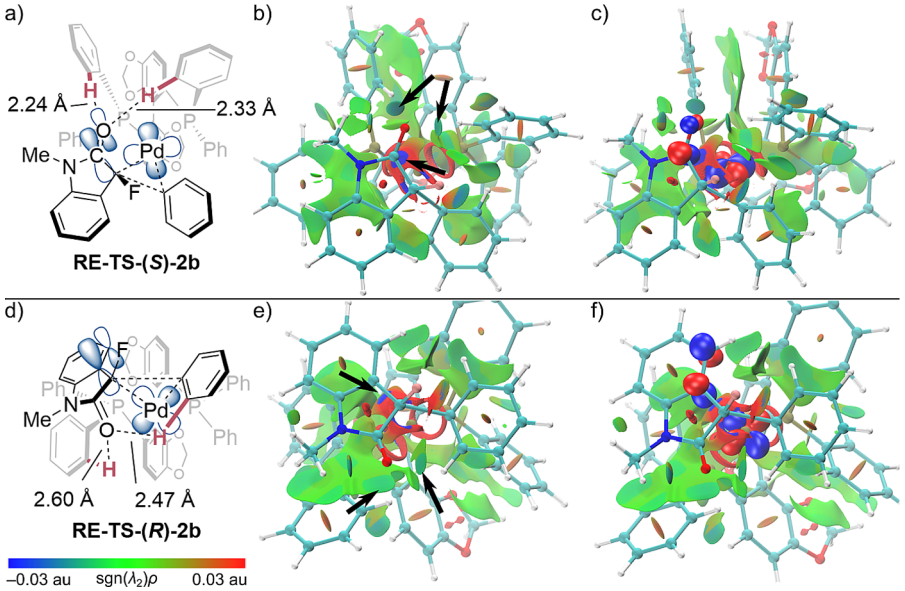

Figure 7. Schematics for the transition state structures (left), NCI plots (center) and overlays of the leading NBOs involved in the $d(\mathrm{Pd}) \rightarrow \pi^*$ interactions (right) for a-c) **RE-TS-(*S*)-2b** and d-f) **RE-TS-(*R*)-2b**. NCI isosurfaces are drawn at $s = 0.05$ au excluding $\rho > 0.05$ au. Grid data were generated with Multiwfn 3.7[51] and visualized with VMD.[52] Black arrows highlight C(aryl)–H···O(carbonyl) and $d(\mathrm{Pd}) \rightarrow \pi^*$ interactions.

energies of either of the two α-C-bound diastereomers. Consistent with the minor diastereomer forming the major enantiomer of the product, the free energy barriers to reductive elimination to form the major product enantiomers (*S*)-**4a** and (*S*)-**4b** from ***pro*-(*S*)-2a** and ***pro*-(*S*)-2b** were calculated to be 22.5 and 21.7 kcal/mol, respectively, while those to elimination to form the minor product enantiomers (*R*)-**4a** and (*R*)-**4b** from ***pro*-(*R*)-2a** and ***pro*-(*R*)-2b** were both calculated to be 26.2 kcal/mol. These computed barriers agree well with the experimentally determined rates of reductive elimination of **2a** ($\Delta G^{\ddagger}_{\mathrm{expt}}$(***pro*-(*S*)-2a**) = 23.7, $\Delta G^{\ddagger}_{\mathrm{expt}}$(***pro*-(*R*)-2a**) = 26.6 kcal/mol) and support the faster rates of reductive elimination observed from phenyl complex **2b** than from 4-cyanophenyl complex **2a**.

The free energy barriers for the isomerization from the α-C-bound isomers ***pro*-(*R*)** and ***pro*-(*S*)** to the corresponding O-bound enolate isomers **κO1** and **κO2** were calculated to be 22–25 kcal/mol. These values are close to the calculated barriers for reductive elimination to form the major enantiomers of the products ((*S*)-**4a**–**b**) and are consistent with the comparable rates of epimerization and reductive elimination to form this enantiomer determined experimentally.[48] Simulations were conducted to determine the *ee* values of α-aryl fluorooxindoles **4a** and **4b** that would result from the reaction of a 1:1 mixture of the corresponding diastereomeric complexes ***pro*-(*R*)-2a,b** and ***pro*-(*S*)-2a,b** with rate constants from the computed free-energy barriers of isomerization and reductive elimination. The simulated *ee* values were found to be 87% and 94% for **4a** and **4b**, respectively, which are well within error of the experimentally observed values of 93% and 95% (see the SI for a discussion on the effects of the small differences in free energy barriers on this value). Altogether, these results support our conclusion that the reductive elimination step has the greatest influence on enantioselectivity and that the minor observed diastereomer forms the major enantiomer of the coupled product.

https://doi.org/10.1021/jacs.1c05346
J. Am. Chem. Soc. 2021, 143, 11741–11750

Further inspection of the calculated transition-state structures for reductive elimination revealed close contacts between the oxygen atom in the carbonyl of the fluorooxindole fragment and several aryl C−H bonds (r = 2.24−2.60 Å; $R_{vdW}(O)$ + $R_{vdW}(H)$[49] = 2.62 Å). These contacts in the transition state to give the major product enantiomer (**RE-TS-(*S*)**; 2.24−2.33 Å; Figure 7a) were shorter than those in the transition state to give the minor enantiomer (**RE-TS-(*R*)**; 2.47−2.60 Å; Figure 7d). Zhou and co-workers previously proposed that such C(aryl)−H···O(carbonyl) interactions were attractive and responsible for the high enantioselectivities observed in their Pd-catalyzed asymmetric arylation of silyl ketene acetals and enol ethers.[32,33]

To probe these close contacts further, we used Noncovalent Interaction (NCI) analysis.[50] This analysis reveals regions of a molecule engaged in noncovalent interactions when both the electron density ρ and reduced density gradient $s = 1/(2(3\pi^2)^{1/3})|\nabla\rho|/\rho^{4/3}$ are near 0. NCI analysis further classifies these regions by the sign of the second eigenvalue λ_2 of the Hessian of ρ as either stabilizing and bonding-like ($\lambda_2 < 0$, colored blue), destabilizing and nonbonded ($\lambda_2 > 0$, colored red), or due to van der Waals interactions ($\lambda_2 \sim 0$, colored green). Regions with larger ρ are considered to represent stronger interactions and are represented visually by more saturated reds and blues.

The NCI plots of structures **RE-TS-(*S*)** and **RE-TS-(*R*)** for phenylpalladium enolate complex **2b** (Figure 7b,e, respectively) display blue-green isosurfaces between the aforementioned C(aryl)−H bonds and the carbonyl oxygen atom of the fluorooxindole fragment, indicating attractive interactions. These interactions are more prominent (darker blue) in the transition state to give the major product enantiomer (**RE-TS-(*S*)-2b**) than in that to give the minor enantiomer (**RE-TS-(*R*)-2b**). While these differences may influence the relative stabilities of the two transition states, the NCI plots also reveal much more prominent, bonding-like interactions between the fluorooxindole fragment and the Pd center. In **RE-TS-(*S*)-2b**, this region is positioned between the Pd center and the carbonyl carbon, while in **RE-TS-(*R*)-2b** it is positioned similarly between the Pd center and one of the carbons of the aryl ring of the fluorooxindole fragment. Notably, these regions were present in neither the starting nor final ground-state complexes (see the SI). We hypothesized that these regions correspond to donor−acceptor interactions between d orbitals on the Pd center and the C=O* antibonding orbital of the carbonyl in the case of **RE-TS-(*S*)-2b** and a π* orbital of the aryl ring in the case of **RE-TS-(*R*)-2b**. Because carbonyl groups are typically more electrophilic than aromatic rings, this interaction should be more stabilizing in **RE-TS-(*S*)-2b** than in **RE-TS-(*R*)-2b**.

To evaluate these hypotheses further, we analyzed the second-order Natural Bond Orbital (NBO) interactions of **RE-TS-(*S*)-2b** and **RE-TS-(*R*)-2b**.[53,54] Second-order NBO interactions quantitatively describe the electronic stabilization resulting from donation of a mostly occupied NBO into another, mostly unoccupied, NBO. Analysis of the donor−acceptor interactions between all (partially) occupied d orbitals of the Pd center and the NBO-localized fluorooxindole C=O* orbital (**RE-TS-(*S*)-2b**; Figure 7c) or the proximal C=C* orbital of the fluorooxindole aryl ring (**RE-TS-(*R*)-2b**; Figure 7f) revealed interaction energies of 8.7 and 3.4 kcal/mol, respectively. These energies are consistent with our hypothesis that the interaction is more stabilizing in the transition state to give the major product enantiomer than in that to give the minor product enantiomer.

This interaction is reflected further in the NAO-based Wiberg bond indices[55] (WBIs) between the Pd center and the relevant atoms of the π* orbitals of the fluorooxindole fragment across the reaction coordinate (Figure 8, gold dotted line). As the

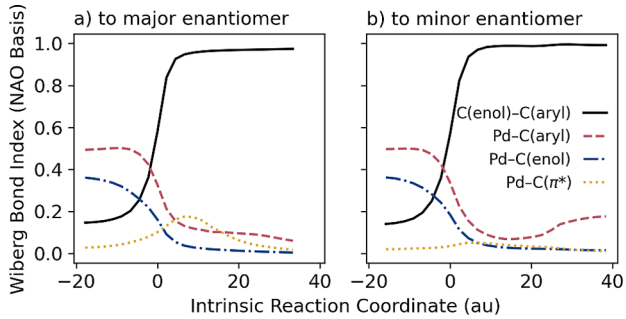

Figure 8. Wiberg bond indices across the intrinsic reaction coordinate for reductive elimination from ***pro*-(*S*)-rot-2b**. IRC = 0 corresponds to the transition state along the path. (a) WBIs along the path to give the major product enantiomer (encountering **RE-TS-(*S*)-2b**). Pd−C(π*) corresponds to the WBI between the Pd center and the C of the enolate C=O. (b) WBIs along the path to give the minor product enantiomer (encountering **RE-TS-(*R*)-2b**). Pd−C(π*) corresponds to the WBI between the Pd center and the nearest C of the phenyl ring of the fluorooxindole fragment. The rising Pd−C(aryl) WBI near the end of the reaction coordinate corresponds to the formation of the product η^2-arene complex **pdt-(*R*)-2b**.

reaction proceeds from the starting complexes ***pro*-(*S*)-rot-2b** and ***pro*-(*R*)-rot-2b**, the WBIs increase to maxima just after the transition state (WBI = 0.175 and 0.052 for **RE-TS-(*S*)-2b** and **RE-TS-(*R*)-2b**, respectively) and then decrease until they reach the product η^2-arene complexes **pdt-(*S*)-2b** and **pdt-(*R*)-2b**. Thus, these interactions arise exclusively in the transition state and are not present in the starting and product complexes. Taken together, these results strongly suggest that d(Pd) → π* interactions are responsible for the stereoselectivity of the reductive elimination step in complexes **2a**−**b**.

4. Kinetic Analysis of the Catalytic Reaction. Having demonstrated that (*S*)-SEGPHOS-ligated fluoroenolate complexes **2a** and **2b** undergo reductive elimination to form α-arylated products in high yields and enantioselectivities, we sought to assess the intermediacy and potential accumulation of these complexes in the catalytic coupling reaction of aryl triflates **7a** and **7b** and fluorooxindole **3** with K_3PO_4 as a base (Scheme 4).[19] When ((*S*)-SEGPHOS)$_2$Pd(0) (**8**) was used as the catalyst precursor, the enantioselectivities of the arylations with aryl triflates **7a** and **7b** (94% and 96%, respectively) matched those obtained for the stoichiometric reductive eliminations from **2a** and **2b** (*vide supra*).

Phenylpalladium fluoroenolate complex **2b** was not detected by $^{19}F\{^{31}P\}$ or $^{31}P\{^{1}H\}$ NMR spectroscopy in an aliquot of the reaction mixture of the arylation of fluorooxindole **3** with phenyl triflate (**7b**) catalyzed by *bis*-(*S*)-SEGPHOS-ligated Pd(0) complex **8** after 1 h (~4% conversion). Instead, complex **8** and free SEGPHOS were the only phosphine-containing species detected in solution by $^{31}P\{^{1}H\}$ NMR spectroscopy (see the SI). This result suggests that ligand dissociation to form (SEGPHOS)Pd(0) or the subsequent oxidative addition of aryl triflate is the turnover-limiting step of the catalytic reaction when **8** is used as the precatalyst.

To probe this hypothesis further, we measured the initial rates of formation of arylated product **4b** while systematically varying

https://doi.org/10.1021/jacs.1c05346
J. Am. Chem. Soc. 2021, 143, 11741−11750

Scheme 4. Catalytic Arylation of 3 with Aryl Triflates[a,b,c]

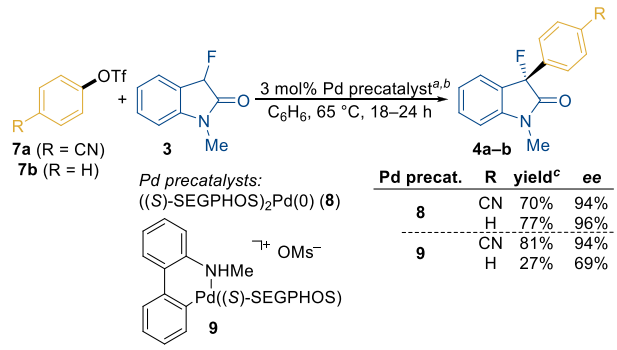

Pd precat.	R	yield[c]	ee
8	CN	70%	94%
	H	77%	96%
9	CN	81%	94%
	H	27%	69%

[a]Aryl triflate (0.100 mmol), **3** (0.200 mmol), K_3PO_4 (0.300 mmol), **8** (0.0030 mmol), (*S*)-SEGPHOS (0.0015 mmol). [b]Aryl triflate (0.100 mmol), **3** (0.200 mmol), K_3PO_4 (0.300 mmol), **9** (0.0030 mmol), 2,6-lutidine (0.018 mmol). [c]Yields determined by quantitative ^{19}F NMR spectroscopy.

the initial concentrations of each component. As shown in Figure 9, the catalytic coupling reaction was first-order in the

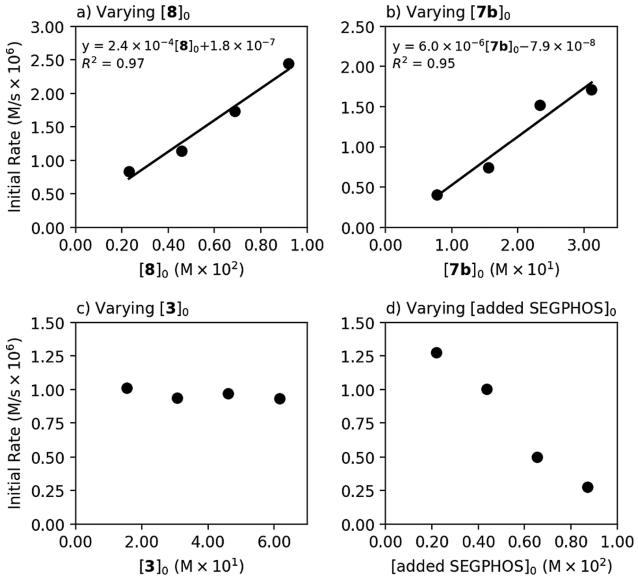

Figure 9. Initial rates of the reaction of phenyl triflate (**7b**) with fluorooxindole **3** catalyzed by ((*S*)-SEGPHOS)$_2$Pd(0) (**8**) vs varying initial concentrations of (a) precatalyst **8**; (b) aryl triflate **7b**; (c) fluorooxindole **3**; and (d) added SEGPHOS. Baseline conditions: **7b** (0.100 mmol, 0.153 M), **3** (0.200 mmol), K_3PO_4 (0.300 mmol), **8** (3.0 mol %), (*S*)-SEGPHOS (1.5 mol %). See the SI for details.

concentrations of precatalyst **8** and aryl triflate **7b**, zero-order in the concentration of fluorooxindole **3**, and inverse order in the concentration of added (*S*)-SEGPHOS. These orders are consistent with turnover-limiting oxidative addition after reversible dissociation of the diphosphine. Moreover, the initial rates of formation of product **4b** were slower than the initial rate that would be observed if reductive elimination from phenylpalladium fluoroenolate complex **2b** were the turnover-limiting step of the reaction (hypothetical $k_{init,RE} = 1.2 \times 10^{-5}$ M·s^{-1} with 3.0 mol % **2b**). Thus, complex **2b** is kinetically competent to be an intermediate in the formation of **4b** under catalytic conditions, but does not accumulate in the catalytic reaction under these conditions.

In contrast to phenyl complex **2b**, the 4-cyanophenyl complex **2a** was detected in the reaction of electron-deficient 4-cyanophenyl triflate (**7a**) with Pd(0) complex **8** as the precatalyst (~50% of the loading of **8** as determined by $^{19}F\{^{31}P\}$ NMR spectroscopy). *Bis*-(*S*)-SEGPHOS complex **8** was also detected in the $^{31}P\{^{1}H\}$ spectrum of this reaction. We hypothesized that the different resting states for the reactions of aryl triflates **7a** and **7b** resulted from the faster oxidative addition of electron-deficient 4-cyanophenyl triflate (**7a**) than that of the more electron-rich phenyl triflate (**7b**). While the oxidative addition step in the reaction of the more electron-rich aryl triflate **7b** was slow enough relative to the reductive elimination from the intermediate fluoroenolate complex **2b** that oxidative addition was the turnover-limiting step in the catalytic reaction, the oxidative addition step in the reaction of the more electron-deficient aryl triflate **7a** was fast enough to be competitive with reductive elimination from the intermediate fluoroenolate complex **2a**, leading to the observation of both palladium(0) complex **8** and fluoroenolate complex **2a** in the reaction of **7a**.

We reasoned that maintaining a 1:1 ratio of SEGPHOS and Pd would mitigate the accumulation of the *bis*-(*S*)-SEGPHOS Pd(0) complex **8** and facilitate the oxidative addition step, thereby causing reductive elimination from the fluoroenolate complex **2a** to be the turnover-limiting step in the catalytic reaction of 4-cyanophenyl triflate (**7a**). After some experimentation, we found that fluoroenolate complex **2a** was the dominant phosphine-containing species in solution for the reaction of **7a** with fluorooxindole **3**, as determined by $^{31}P\{^{1}H\}$ NMR spectroscopy, when the (*S*)-SEGPHOS-ligated palladacycle **9** was used as the precatalyst (see the SI).

Analysis of the initial rates of the formation of α-aryl-oxindole **4a** during the reaction of 4-cyanophenyl triflate (**7a**), fluorooxindole **3**, and precatalyst **9** revealed a zero-order dependence of the rate of the catalytic reaction on the concentrations of aryl triflate **7a** and fluorooxindole **3** and a first-order dependence on the concentration of precatalyst **9**, consistent with turnover-limiting reductive elimination from the resting-state fluoroenolate complex **2a** (Figure 10). The k_{obs} determined from a plot of the initial rates of formation of arylated product **4a** vs the loading of precatalyst **9** was 6.9×10^{-4} s^{-1}, which is close to the observed rate constant for reductive elimination from **2a** measured in the stoichiometric experiments (8.6×10^{-4} s^{-1}, *vide supra*).[56] The *ee* value of the resulting arylated product **4a** was also 94%, which matches that obtained from thermolysis of **2a** or in reactions catalyzed by ((*S*)-SEGPHOS)$_2$Pd(0) (**8**). Taken together, these results directly implicate arylpalladium fluoroenolate complexes **2a** and **2b** as the species that form the C−C bond and control enantioselectivity during the formation of **4a** and **4b** under catalytic conditions.[57]

CONCLUSION

In summary, we have prepared a series of diphosphine-ligated, arylpalladium α-C-bound fluorooxindole complexes, including two complexes bearing (*S*)-SEGPHOS as the ancillary ligand, that begin to reveal the origins of enantioselectivity in the enantioselective α-arylation of carbonyl compounds. These complexes undergo reductive elimination to form α-aryl-α-fluorooxindoles in quantitative yields. The SEGPHOS-ligated arylpalladium fluorooxindole complexes **2a**−**b** formed the coupled products with *ee* values that matched those obtained in the Pd-catalyzed coupling of aryl triflates with fluorooxindole **3**, and **2a** was directly observed in the crude catalytic reaction

https://doi.org/10.1021/jacs.1c05346
J. Am. Chem. Soc. 2021, 143, 11741−11750

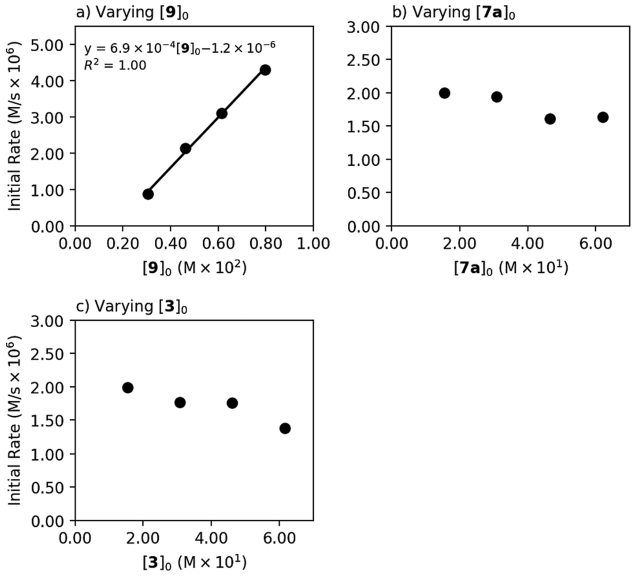

Figure 10. Initial rates of the reaction of aryl triflate **7a** with fluorooxindole **3** catalyzed by precatalyst **9** vs varying initial concentrations of (a) precatalyst **9**; (b) aryl triflate **7a**; and (c) fluorooxindole **3**. Baseline conditions: **7a** (0.100 mmol, 0.153 M), **3** (0.200 mmol), K_3PO_4 (0.300 mmol), **9** (3.0 mol %), and 2,6-lutidine (12 mol %). See the SI for details.

mixture. These experiments established the relevance of these complexes to catalysis and the origins of enantioselectivity. Epimerization between the two diastereomers of the SEGPHOS-ligated complexes was observed directly and was shown to be faster than reductive elimination, demonstrating that the enantioselectivity of the reaction is determined by the relative rates of reductive elimination from the two diastereomers. Computational analysis suggests that the difference in energy between the two diastereomeric transition states to reductive elimination is due to interactions between the carbonyl oxygen atom of the fluorooxindole fragment with the aryl C−H bonds of the SEGPHOS ligand, as well as donor−acceptor interactions between the Pd center and π^* orbitals of the fluoroenolate fragment.

Given that arylpalladium fluoroalkyl complexes undergo reductive elimination more slowly than their nonfluorinated counterparts,[28,37] two scenarios for the enantioselective arylation of nonfluorinated enolates are possible in light of the current work. First, if the difference in the rate of the isomerization between the O- and C-bound forms of the fluorinated and nonfluorinated enolate complexes is similar or greater than the difference in the rate of reductive elimination of the two types of complexes, then reductive elimination would remain the principal determinant of enantioselectivity. In this case, enantioselectivities from the arylations of nonfluorinated enolates could be enhanced by designing systems to facilitate the aforementioned C−H···O and $d \rightarrow \pi^*$ interactions. If isomerization between the O- and C-bound forms of the nonfluorinated enolates is significantly slower than reductive elimination, then the formation of the diastereomeric enolate complexes would control enantioselectivity, and factors to form one C-bound diastereomer over the other would need to be developed. To this end, increasing the size of the substituent on the α-carbon while maintaining its electron-withdrawing nature could enable the observation of both C-bound and O-bound arylpalladium enolate species and the measurement of the rates of conversion among them. Studies to assess the relationship of these conclusions to the reactions of enolates lacking fluorine and to design further enantioselective fluoroalkylations are in progress.

■ ASSOCIATED CONTENT

Supporting Information

The Supporting Information is available free of charge at https://pubs.acs.org/doi/10.1021/jacs.1c05346.

Experimental procedures, spectral data, reaction time course data, and computational procedures (PDF)

Molecular coordinates of computed structures (XYZ)

Accession Codes

CCDC 2087689 contains the supplementary crystallographic data for this paper. These data can be obtained free of charge via www.ccdc.cam.ac.uk/data_request/cif, or by emailing data_request@ccdc.cam.ac.uk, or by contacting The Cambridge Crystallographic Data Centre, 12 Union Road, Cambridge CB2 1EZ, UK; fax: +44 1223 336033.

■ AUTHOR INFORMATION

Corresponding Author

John F. Hartwig − *Department of Chemistry, University of California, Berkeley, California 94702, United States;* orcid.org/0000-0002-4157-468X; Email: jhartwig@berkeley.edu

Author

Eric D. Kalkman − *Department of Chemistry, University of California, Berkeley, California 94702, United States;* orcid.org/0000-0002-9365-1261

Complete contact information is available at: https://pubs.acs.org/10.1021/jacs.1c05346

Notes

The authors declare no competing financial interest.

■ ACKNOWLEDGMENTS

We thank the NSF (CHE-1955635) for support of this work. We also thank the College of Chemistry's NMR, Molecular Graphics and Computation, and Small Molecule X-ray Crystallography (CheXray) facilities and the Lawrence Berkeley National Lab Catalysis Facility for resources provided and the staff for their assistance. In particular, we thank Dr. Hasan Celik for his assistance and advice in acquiring nonstandard heteronuclear spectra (*e.g.*, inverse-gated $^{19}F\{^{31}P\}$) and in characterizing fluorine-containing compounds; Dr. Dave Small for his assistance planning and validating DFT calculations and NCI analyses; and Dr. Nicholas Settineri for acquiring and processing XRD structures. Instruments in the CoC-NMR are supported in part by NIH S10OD024998. The Molecular Graphics and Computation Facility is supported by NIH S10OD023532. CheXray is supported by NIH S10-RR027172.

■ REFERENCES

(1) Palucki, M.; Buchwald, S. L. , Palladium-Catalyzed α-Arylation of Ketones. *J. Am. Chem. Soc.* **1997**, *119*, 11108−11109.

(2) Hamann, B. C.; Hartwig, J. F. Palladium-Catalyzed Direct α-Arylation of Ketones. Rate Acceleration by Sterically Hindered Chelating Ligands and Reductive Elimination from a Transition Metal Enolate Complex. *J. Am. Chem. Soc.* **1997**, *119*, 12382−12383.

(3) Satoh, T.; Kawamura, Y.; Miura, M.; Nomura, M. , Palladium-Catalyzed Regioselective Mono- and Diarylation Reactions of 2-Phenylphenols and Naphthols with Aryl Halides. *Angew. Chem., Int. Ed. Engl.* **1997**, *36*, 1740−1742.
(4) Muratake, H.; Natsume, M. , Palladium-Catalyzed Intramolecular α-Arylation of Aliphatic Ketones. *Tetrahedron Lett.* **1997**, *38*, 7581−7582.
(5) Muratake, H.; Hayakawa, A.; Natsume, M. , A Novel Phenol-Forming Reaction for Preparation of Benzene, Furan, and Thiophene Analogs of CC-1065/Duocarmycin Pharmacophores. *Tetrahedron Lett.* **1997**, *38*, 7577−7580.
(6) Culkin, D. A.; Hartwig, J. F. , Palladium-Catalyzed α-Arylation of Carbonyl Compounds and Nitriles. *Acc. Chem. Res.* **2003**, *36*, 234−45.
(7) Prim, D.; Marque, S.; Gaucher, A.; Campagne, J.-M. In *Organic Reactions*, Vol. *76*; Denmark, S. E. et al., Eds John Wiley & Sons, Inc.: Hoboken, NJ, 2012; pp 50−276.
(8) Magano, J.; Dunetz, J. R. , Large-Scale Applications of Transition Metal-Catalyzed Couplings for the Synthesis of Pharmaceuticals. *Chem. Rev.* **2011**, *111*, 2177−250.
(9) Hao, Y.-J.; Hu, X.-S.; Zhou, Y.; Zhou, J.; Yu, J.-S. , Catalytic Enantioselective α-Arylation of Carbonyl Enolates and Related Compounds. *ACS Catal.* **2020**, *10*, 955−993.
(10) Åhman, J.; Wolfe, J. P.; Troutman, M. V.; Palucki, M.; Buchwald, S. L. , Asymmetric Arylation of Ketone Enolates. *J. Am. Chem. Soc.* **1998**, *120*, 1918−1919.
(11) Lee, S.; Hartwig, J. F. Improved Catalysts for the Palladium-Catalyzed Synthesis of Oxindoles by Amide α-Arylation. Rate Acceleration, Use of Aryl Chloride Substrates, and a New Carbene Ligand for Asymmetric Transformations. *J. Org. Chem.* **2001**, *66*, 3402−15.
(12) Hamada, T.; Chieffi, A.; Ahman, J.; Buchwald, S. L. , An Improved Catalyst for the Asymmetric Arylation of Ketone Enolates. *J. Am. Chem. Soc.* **2002**, *124*, 1261−8.
(13) Liao, X.; Weng, Z.; Hartwig, J. F. , Enantioselective α-Arylation of Ketones with Aryl Triflates Catalyzed by Difluorphos Complexes of Palladium and Nickel. *J. Am. Chem. Soc.* **2008**, *130*, 195−200.
(14) Garcia-Fortanet, J.; Buchwald, S. L. , Asymmetric Palladium-Catalyzed Intramolecular α-Arylation of Aldehydes. *Angew. Chem., Int. Ed.* **2008**, *47*, 8108−11.
(15) Taylor, A. M.; Altman, R. A.; Buchwald, S. L. , Palladium-Catalyzed Enantioselective α-Arylation and α-Vinylation of Oxindoles Facilitated by an Axially Chiral P-Stereogenic Ligand. *J. Am. Chem. Soc.* **2009**, *131*, 9900−1.
(16) Zhou, J. , Recent Developments in Asymmetric Coupling of Enolates. *Synlett* **2012**, *2012*, 1−5.
(17) Nareddy, P.; Mantilli, L.; Guenee, L.; Mazet, C. , Atropoisomeric (P,N) Ligands for the Highly Enantioselective Pd-Catalyzed Intramolecular Asymmetric α-Arylation of α-Branched Aldehydes. *Angew. Chem., Int. Ed.* **2012**, *51*, 3826−31.
(18) Jiao, Z.; Beiger, J. J.; Jin, Y.; Ge, S.; Zhou, J. S.; Hartwig, J. F. , Palladium-Catalyzed Enantioselective α-Arylation of α-Fluoroketones. *J. Am. Chem. Soc.* **2016**, *138*, 15980−15986.
(19) Jin, Y.; Chen, M.; Ge, S.; Hartwig, J. F. , Palladium-Catalyzed, Enantioselective α-Arylation of α-Fluorooxindoles. *Org. Lett.* **2017**, *19*, 1390−1393.
(20) Rao, X.; Li, N.; Bai, H.; Dai, C.; Wang, Z.; Tang, W. , Efficient Synthesis of (−)-Corynoline by Enantioselective Palladium-Catalyzed α-Arylation with Sterically Hindered Substrates. *Angew. Chem., Int. Ed.* **2018**, *57*, 12328−12332.
(21) Jette, C. I.; Geibel, I.; Bachman, S.; Hayashi, M.; Sakurai, S.; Shimizu, H.; Morgan, J. B.; Stoltz, B. M. , Palladium-Catalyzed Construction of Quaternary Stereocenters by Enantioselective Arylation of gamma-Lactams with Aryl Chlorides and Bromides. *Angew. Chem., Int. Ed.* **2019**, *58*, 4297−4301.
(22) Chieffi, A.; Kamikawa, K.; Ahman, J.; Fox, J. M.; Buchwald, S. L. , Catalytic Asymmetric Vinylation of Ketone Enolates. *Org. Lett.* **2001**, *3*, 1897−900.
(23) Liu, X.; Hartwig, J. F. , Palladium-Catalyzed α-Arylation of Azlactones to Form Quaternary Amino Acid Derivatives. *Org. Lett.* **2003**, *5*, 1915−8.
(24) Jiao, Z.; Chee, K. W.; Zhou, J. S. , Palladium-Catalyzed Asymmetric α-Arylation of Alkylnitriles. *J. Am. Chem. Soc.* **2016**, *138*, 16240−16243.
(25) Huang, X.; Oh, W.; Zhou, J. S. , Palladium-Catalyzed Enantioselective Arylation of Racemic Ketones to Form Bridged Bicycles via Dynamic Kinetic Resolution. *Angew. Chem., Int. Ed.* **2018**, *57*, 7673−7677.
(26) Ostrowska, S.; Scattolin, T.; Nolan, S. P. , N-Heterocyclic carbene complexes enabling the α-arylation of carbonyl compounds. *Chem. Commun.* **2021**, *57*, 4354−4375.
(27) Culkin, D. A.; Hartwig, J. F. , C-C Bond-Forming Reductive Elimination of Ketones, Esters, and Amides from Isolated Arylpalladium(II) Enolates. *J. Am. Chem. Soc.* **2001**, *123*, 5816−7.
(28) Culkin, D. A.; Hartwig, J. F. Carbon-Carbon Bond-Forming Reductive Elimination from Arylpalladium Complexes Containing Functionalized Alkyl Groups. Influence of Ligand Steric and Electronic Properties on Structure, Stability, and Reactivity. *Organometallics* **2004**, *23*, 3398−3416.
(29) Kawatsura, M.; Hartwig, J. F. , Simple, Highly Active Palladium Catalysts for Ketone and Malonate Arylation: Dissecting the Importance of Chelation and Steric Hindrance. *J. Am. Chem. Soc.* **1999**, *121*, 1473−1478.
(30) Liu, X.; Hartwig, J. F. Palladium-Catalyzed Arylation of Trimethylsilyl Enolates of Esters and Imides. High Functional Group Tolerance and Stereoselective Synthesis of α-Aryl Carboxylic Acid Derivatives. *J. Am. Chem. Soc.* **2004**, *126*, 5182−91.
(31) Huang, Z.; Liu, Z.; Zhou, J. S. , An Enantioselective, Intermolecular α-Arylation of Ester Enolates to Form Tertiary Stereocenters. *J. Am. Chem. Soc.* **2011**, *133*, 15882−5.
(32) Huang, Z.; Chen, Z.; Lim, L. H.; Quang, G. C.; Hirao, H.; Zhou, J. S. , Weak Arene C−H···O Hydrogen Bonding in Palladium-Catalyzed Arylation and Vinylation of Lactones. *Angew. Chem., Int. Ed.* **2013**, *52*, 5807−12.
(33) Huang, Z. Y.; Lim, L. H.; Chen, Z. L.; Li, Y. X.; Zhou, F.; Su, H. B.; Zhou, J. R. , Arene CH−O Hydrogen Bonding: A Stereocontrolling Tool in Palladium-Catalyzed Arylation and Vinylation of Ketones. *Angew. Chem., Int. Ed.* **2013**, *52*, 4906−4911.
(34) Yang, J.; Zhou, J. , A general method for asymmetric arylation and vinylation of silyl ketene acetals. *Org. Chem. Front.* **2014**, *1*, 365−367.
(35) Kirker, G. W.; Bakac, A.; Espenson, J. H. , Homolysis and Acidolysis Reactions of (α-Hydroxyalkyl)- and (α-Alkoxyalkyl)-chromium(III) Complexes: Kinetics, Steric Effects, and Bond Energies. *J. Am. Chem. Soc.* **1982**, *104*, 1249−1255.
(36) Blau, R. J.; Espenson, J. H.; Bakac, A. , Kinetic Study of the Reaction of Aquochromium(II) Ions with Benzyl Radicals in Aqueous Solutions: Thermodynamics of the Chromium−Carbon Bond. *Inorg. Chem.* **1984**, *23*, 3526−3528.
(37) Albéniz, A. C.; Casares, J. A., Chapter One - Palladium-Mediated Organofluorine Chemistry. In *Adv. Organomet. Chem.*, Pérez, P. J., Ed. Academic Press: 2014; Vol. *62*, pp 1−110.
(38) In the case of CN-substituted complex **2a**, the fact that equilibration is slow enough to observe over the course of the thermolysis reaction means that the reaction is not goverened by traditional Curtin-Hammett kinetics, which require a fast equilibrium between diastereomers. However, the barriers to reductive elimination remain the most significant driver of enantioselectivity. See the SI for a more detailed kinetic treatment.
(39) Hoops, S.; Sahle, S.; Gauges, R.; Lee, C.; Pahle, J.; Simus, N.; Singhal, M.; Xu, L.; Mendes, P.; Kummer, U. , COPASI—a COmplex PAthway SImulator. *Bioinformatics* **2006**, *22*, 3067−74.
(40) Driver, M. S.; Hartwig, J. F. , Carbon−Nitrogen-Bond-Forming Reductive Elimination of Arylamines from Palladium(II) Phosphine Complexes. *J. Am. Chem. Soc.* **1997**, *119*, 8232−8245.
(41) Mann, G.; Barañano, D.; Hartwig, J. F.; Rheingold, A. L.; Guzei, I. A. Carbon−Sulfur Bond-Forming Reductive Elimination Involving sp-, sp^2-, and sp^3-Hybridized Carbon. Mechanism, Steric Effects, and

Electronic Effects on Sulfide Formation. *J. Am. Chem. Soc.* **1998**, *120*, 9205−9219.
(42) Widenhoefer, R. A.; Buchwald, S. L. , Electronic Dependence of C-O Reductive Elimination from Palladium (Aryl)neopentoxide Complexes. *J. Am. Chem. Soc.* **1998**, *120*, 6504−6511.
(43) Hartwig, J. F. , Electronic Effects on Reductive Elimination to Form Carbon-Carbon and Carbon-Heteroatom Bonds from Palladium(II) Complexes. *Inorg. Chem.* **2007**, *46*, 1936−47.
(44) Gu, Y.; Leng, X.; Shen, Q. , Cooperative dual palladium/silver catalyst for direct difluoromethylation of aryl bromides and iodides. *Nat. Commun.* **2014**, *5*, 5405.
(45) Arlow, S. I.; Hartwig, J. F. , Synthesis, Characterization, and Reactivity of Palladium Fluoroenolate Complexes. *J. Am. Chem. Soc.* **2017**, *139*, 16088−16091.
(46) Hansch, C.; Leo, A.; Taft, R. W. , A Survey of Hammett Substituent Constants and Resonance and Field Parameters. *Chem. Rev.* **1991**, *91*, 165−195.
(47) Widenhoefer, R. A.; Zhong, H. A.; Buchwald, S. L. , Direct Observation of C−O Reductive Elimination from Palladium Aryl Alkoxide Complexes to Form Aryl Ethers. *J. Am. Chem. Soc.* **1997**, *119*, 6787−6795.
(48) The higher calculated barrier of isomerization from ***pro*-(*S*)-2a** to ***pro*-(*R*)-2a** relative to the barrier of reductive elimination from ***pro*-(*S*)-2a** is within the error typically expected for DFT calculations. See the SI for a comparison of different functionals.
(49) Bondi, A. , van der Waals Volumes and Radii. *J. Phys. Chem.* **1964**, *68*, 441−451.
(50) Johnson, E. R.; Keinan, S.; Mori-Sanchez, P.; Contreras-Garcia, J.; Cohen, A. J.; Yang, W. , Revealing Noncovalent Interactions. *J. Am. Chem. Soc.* **2010**, *132*, 6498−506.
(51) Lu, T.; Chen, F. , Multiwfn: a multifunctional wavefunction analyzer. *J. Comput. Chem.* **2012**, *33*, 580−92.
(52) Humphrey, W.; Dalke, A.; Schulten, K. , VMD: Visual molecular dynamics. *J. Mol. Graphics* **1996**, *14*, 33−38.
(53) Reed, A. E.; Curtiss, L. A.; Weinhold, F. , Intermolecular Interactions from a Natural Bond Orbital, Donor-Acceptor Viewpoint. *Chem. Rev.* **1988**, *88*, 899−926.
(54) Glendening, E. D.; Landis, C. R.; Weinhold, F. NBO 6.0: natural bond orbital analysis program. *J. Comput. Chem.* **2013**, *34*, 1429−37.
(55) Wiberg, K. B. , Application of the pople-santry-segal CNDO method to the cyclopropylcarbinyl and cyclobutyl cation and to bicyclobutane. *Tetrahedron* **1968**, *24*, 1083−1096.
(56) The negative intercept of the plot of initial rate vs [**9**] (Figure 10a) is likely due to instability of the intermediate arylpalladium triflate complexes or trace impurities in the starting materials, as suggested by the slightly downward-trending rates with increasing loadings of **7a** and **3** (Figure 10b−c).
(57) Unfortunately, when palladacycle **9** was used as a precatalyst for the catalytic reaction of phenyl triflate (**7b**) with fluorooxindole **3**, the yield and *ee* of arylated product **4b** were significantly lower than those from the same reaction using Pd(0) complex **8** as the precatalyst or from thermolysis of (*S*)-SEGPHOS-ligated arylpalladium enolate complex **2b**. We hypothesize the unstable putative arylpalladium triflate complex formed by oxidative addition of **7b** to the unsaturated complex ((*S*)-SEGPHOS)Pd(0) decomposed at the start of the reaction before a sufficient amount of deprotonated **3** could be generated to quench it.

https://doi.org/10.1021/jacs.1c05346
J. Am. Chem. Soc. 2021, 143, 11741−11750